Iterative correction of shocked acetone high-speed PLIF measurements in the Richtmyer-Meshkov instability

J. M. Herzog, A. Ames, C. Noble, J. Oakley, R. Bonazza, D. A. Rothamer
University of Wisconsin, 1500 Engineering Dr., Madison, WI 53706, USA

Corresponding Author's Email Address: jherzog2@wisc.edu

Abstract Experimental investigations of shock-induced turbulent mixing often employ spatially and temporally resolved optical diagnostics such as planar laser-induced fluorescence (PLIF) to observe the mixing process. However, due to the complex dependence of the PLIF signal on local conditions, quantitative interpretation of the PLIF data is difficult. This work investigates the possibility for rigorous interpretation of PLIF imaging data from Richtmyer-Meshkov instability (RMI) experiments by taking local temperature and composition into account to provide a more quantitative estimate of local tracer mole fraction and temperature. A correction strategy is outlined using an adiabatic mixing assumption. The mixing assumption was validated against high-fidelity simulation data from the *Miranda* hydrodynamics code, and the correction strategy was applied to high-speed PLIF data taken following reshock of a perturbed helium-argon interface at Mach 1.8. Comparison to simulation suggests that the adiabatic mixing approximation is valid to within approximately 30 K for the current conditions, and more typically within 20 K, but requires a good estimate of the temperatures of the unmixed helium and argon regions. When applied to experimental data, the correction strategy resulted in significant differences in the span-wise averaged light-gas mole fraction (on the order of 10% absolute throughout much of the profile) compared to a constant-property correction, demonstrating the magnitude of the errors introduced without correcting for these PLIF dependencies.

1 Introduction

Investigation of shock-accelerated mixing requires spatio-temporal measurements of composition in the region of interest. Planar laser-induced fluorescence (PLIF) of a tracer molecule, such as acetone, is often used as a convenient proxy for local composition. However, tracer fluorescence intensity is dependent on local temperature, pressure, and composition. Since the mixing region contains large gradients in both temperature and density after passage of the shock, quantitative interpretation of PLIF images in terms of local composition alone is not straightforward. Accurate determination of composition requires accounting for the spatio-temporal variation in tracer photophysical parameters. In this paper, we apply an iterative correction approach using an adiabatic mixing assumption to account for temperature, species concentration, and Beer-Lambert attenuation of PLIF intensity following reshock in turbulent Richtmyer-Meshkov Instability (RMI) mixing experiments. This procedure is used to improve estimates of mole fraction within the mixing layer, and provides an additional spatially-resolved estimate of temperature.

The iterative PLIF correction approach has been applied successfully before in fuel vapor measurements in rapid compression machines [1] and optically-accessible engines [2, 3] to account for temperature variation throughout fuel jets. Similar to this paper, an adiabatic mixing assumption within the fuel jet was employed to relate equivalence ratio and temperature and allow measurement of both properties. In [1–3] PLIF intensity was

calibrated for equivalence ratio and temperature since quenching behavior of the tracer was not well known at the compositions and conditions encountered. Additionally, in these studies Beer-Lambert attenuation was not corrected as tracer concentrations were sufficiently low that no appreciable absorption was observed.

This paper describes a more general framework for PLIF correction including the effect of Beer-Lambert attenuation and nonuniform photophysical parameters. The adiabatic mixing assumption is outlined in detail and sample calculations for typical conditions observed at the Wisconsin Shock Tube Laboratory (WiSTL) following reshock of a helium-argon interface are provided. Additionally, implications for different gas pairs are discussed, and estimates of acetone photophysical parameters are made. The adiabatic mixing assumption is tested against high-fidelity simulation results calculated with the *Miranda* hydrodynamics code [4]. Finally, the correction is applied to PLIF data taken at WiSTL following reshock of a helium-argon interface, and mole-fraction and estimated temperature are reported. The importance of temperature correction is assessed by comparing mole fractions calculated using the proposed correction to those calculated assuming constant temperature.

2 Iterative PLIF Correction

Tracer PLIF signal intensity S as measured on a camera can be directly related to the product of the local laser fluence E'', tracer number density n, fluorescence quantum yield (FQY) Φ, and absorption cross-section σ [5]. The measured signal relative to a reference condition (denoted by the subscript 0) can thus be written as

$$\frac{S(x)}{S_0} = \frac{n\sigma\Phi}{n_0\sigma_0\Phi_0}\frac{E''}{E_0''} = \frac{n\sigma\Phi}{n_0\sigma_0\Phi_0}\exp\left(-\int_{x_0}^{x} n\sigma\,\mathrm{d}x^\star\right), \tag{1}$$

where the integral in $x^\star$ is taken along the laser path. In RMI experiments, the reference condition is generally chosen above the mixing layer where properties are assumed to be constant [6], and x is is taken along the direction of laser propagation. The local laser fluence is described by the Beer-Lambert law, which is exponential in number density and absorption cross-section as shown in Eq. (1). This equation is explicit in the measured signal intensity, and implicitly contains dependence on local temperature and pressure through the photophysical parameters σ and Φ.

Eq. (1) can be solved exactly for number density for the analysis of PLIF data. Taking the derivative with respect to x (where a single prime $'$ is used to denote the derivative) and dividing by S results in

$$(n\sigma)' + \left(\frac{\Phi'}{\Phi} - \frac{S'}{S}\right)(n\sigma) = (n\sigma)^2, \tag{2}$$

which is a Bernoulli differential equation in the variable $n\sigma$. The particular solution, incorporating the initial condition $n(x_0)\sigma(x_0) = n_0\sigma_0$ and $S(x_0) = S_0$, is

$$\frac{n\sigma}{n_0\sigma_0} = \frac{\Phi_0 S}{\Phi S_0}\left[1 + n_0\sigma_0\int_{x_0}^{x}\frac{S\Phi_0}{S_0\Phi}\,\mathrm{d}x^\star\right]^{-1}. \tag{3}$$

Eq. (3) can be solved directly along the laser beam path if FQY and absorption cross-section are known along the path. In RMI experiments, due to the typically large difference in specific heat ratio between the two fluids at the interface, temperature can

vary significantly along the integral path. In such cases, the FQY and absorption cross-sections are not constant and make the calculation more difficult.

To address this, the local mole fraction can be used to estimate the local temperature and correct for variation in the FQY and absorption cross section. For an ideal gas, the tracer mole fraction is given by

$$\chi = n\frac{k_B T}{p} = \chi_0 \frac{T_0 p}{T p_0}\frac{\sigma_0 \Phi_0 S}{\sigma \Phi S_0}\left[1 + n_0 \sigma_0 \int_{x_0}^{x} \frac{S\Phi_0}{S_0 \Phi}\,\mathrm{d}x^\star\right]^{-1}, \tag{4}$$

where k_B is the Boltzmann constant, and T_0 and p_0 are the temperature and pressure at the reference condition. Normalizing the tracer mole fraction by the mole fraction at the uniform condition results in the seeded gas mole fraction $\zeta = \chi/\chi_0$.

Note that this procedure assumes there are no chemical reactions in the system, and that the acetone mass is constant. In reality, unimolecular decomposition of acetone occurs at a wide range of timescales in inert baths, with measured timescales as short as hundreds of microseconds or less in argon at 1400 K and low pressure [7]. The validity of the constant acetone approximation must be assessed for each individual condition.

2.1 Temperature Estimation

Due to the relatively short time scales involved in the shock-driven mixing process, thermal diffusion is assumed to be negligible and the local temperature is determined by the local mole fraction, where the mixing is assumed to be adiabatic. The enthalpy of the mixture is determined based on a mixing rule and depends on the equation of state used for the calculation. For an ideal gas, the enthalpy of the mixture is simply the mole-fraction weighted average of the pure component enthalpies evaluated at the adiabatic mixture temperature, and the excess enthalpy is zero. For more complicated equations of state the mixture properties must be estimated before calculating the mixture enthalpy.

For an ideal gas, the enthalpy of a mixture of components A and B is assumed to be equal to the average enthalpy of the initially pure fluids, i.e.,

$$\bar{h}(T;\chi) = \chi h_A(T_{0,A}) + (1-\chi)h_B(T_{0,B}), \tag{5}$$

where $\bar{h}$ is the molar-specific mixture enthalpy, h_i is the molar-specific enthalpy of species i, $T_{0,i}$ is the initial unmixed temperature of species i, and T is the adiabatic mixture temperature. Typically enthalpy dependence on pressure is neglected but could be included in the enthalpy departure function of a non-ideal equation of state. In either case, the mixing process is often assumed to be isobaric to first order (*e.g.*, in [8]), and this approximation will be used here as well.

For two monatomic gases at sufficiently low temperatures, such as for the case of helium and argon, the mixture temperature is simply a mole-fraction weighted average. If the assumption of constant specific heat capacity is made for a two fluid mixture with temperatures T_0 and T_1, and both fluids have the same molar-specific heat capacities, then the adiabatic temperature of the binary mixture is

$$T = \frac{\chi c_p T_0 + (1-\chi)c_p T_1}{\chi c_p T_0 + (1-\chi)c_p T_1} = \chi T_0 + (1-\chi)T_1, \tag{6}$$

which is a linear function of the mixing fraction. If the heat capacities are not constant with temperature, or if the two fluids have different specific heats, the adiabatic mixture temperature is not a linear function of mole fraction.

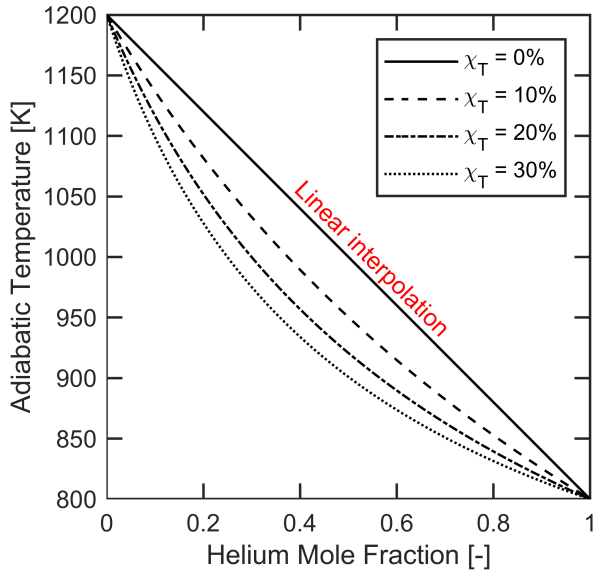

Fig. 1: Adiabatic mixture temperature for helium seeded with acetone (0, 10, 20, and 30% acetone fractions) and argon.

Sample calculations of adiabatic mixture temperature were performed for a typical reshock RMI condition at 16 bar for helium seeded with acetone at an initial temperature of 800 K mixing with argon at an initial temperauture of 1200 K. These conditions are representative of typical reshock conditions for experiments performed at WiSTL. The adiabatic mixture temperatures for this case are shown in Fig. 1 for severval different seeding concentrations of acetone in the helium, ranging from 0 to 30% mole fraciton. The adiabatic temperatures in Fig. 1 are calculated using an ideal gas equation of state that allows for temperature dependent specific heat capacities. In this calculation helium and argon have constant heat capacities since they are both monatomic. However, acetone has a strongly temperature-dependent specific heat capacity. Heat capacities are calculated using the NASA polynomial form with coefficients taken from the LLNL detailed n-heptane reaction mechanism [9].

As already mentioned, for the case of equal and constant specific heats, corresponding to the 0% acetone curve in Fig. 1 the adiatic temperature is a linear function of mole fraction. As the amount of acetone in the helium is increased, the adiabatic temperature versus mole fraction becomes more non-linear due to the difference in the molar specific heat for acetone and due to its dependence on temperature. For a 30% acetone concentration, linearly interpolating temperature between the endpoints instead of accounting appropriately for the differences in specific heats results in a maximum error of about 100 K.

2.2 Photophysical Parameters for Acetone

Acetone absorption cross-section and fluorescence quantum yield measurements at different conditions have been published from several studies [10–12]. In particular a fluorescence quantum yield model has been developed by Thurber [10] and was later calibrated to Rayleigh scattering measurements [13]. Additionally, Koch [11] provided a curve fit for the absorption cross-section of acetone. These models are used to estimate acetone

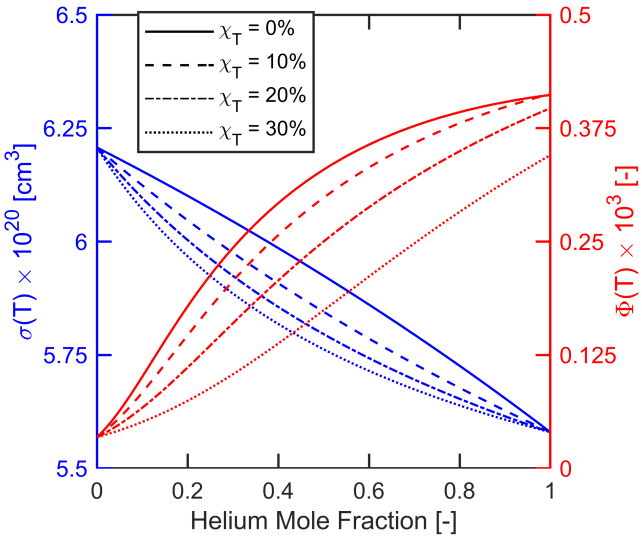

Fig. 2: Fluorescence quantum yield (red) and absorption cross-section (blue) predicted by models from Thurber [10] and Koch [11], respectively, for the adiabatic mixture composition and temperature in Fig. 1.

photophysical parameters for image correction. The FQY model parameters of Koch et al. [13] are used here, but other parameter values or models for FQY could be used in the correction approach.

The local temperature and composition significantly impact the fluorescence quantum yield. Fig. 2 plots the predicted fluorescence quantum yield and absorption cross-section for the adiabatic helium-acetone and argon mixture for an excitation wavelength of 266 nm. The absorption cross-section is dependent on temperature, but only very weakly at 266 nm excitation with less than 15% change between 800 and 1200 K. The fluorescence quantum yield is additionally influenced by local composition. The effect of composition can be observed immediately when the helium mole fraction is one; here increasing tracer concentration shows a slight decrease in FQY predicted by the model. Though this calculation is focused only on helium, argon, and acetone, the presence of oxygen or other species could additionally have a strong quenching effect for some tracers that must be taken into consideration. This is particularly important when air is introduced into the experiment as oxygen tends to quench fluorescence. Since quenching data for argon are not available, its quenching effect is assumed to be similar to that of N_2 for the present calculations.

3 Validation of Mixing Model & Correction

3.1 Simulation Setup

The validity of the iterative correction procedure is tested against data from a simulated shock-accelerated interface, namely the propagation of a $M = 1.8$ shock wave from pure helium into pure argon across a quiescent interface with broadband 3-D sinusoidal perturbations. For simplicity this simulation does not include acetone. The simulation was performed with the *Miranda* hydrodynamics code [4] in a $0.25 \times 0.25 \times 2.5\,\mathrm{m}$ rectilinear domain with nx = ny = 128, nz = 1280 equispaced nodes, periodic boundary conditions in the x and y directions, and a reflective boundary condition 1.5 m below the initial

location of the interface. *Miranda* calculates the solution of the Navier-Stokes equations for Newtonian fluids by casting the constitutive equations (7)–(9) in conservative form, with spatial derivatives approximated by a 10th-order-accurate compact finite difference scheme, and time advancement via a five-step, fourth-order Runge-Kutta integrator.

$$\frac{\partial \rho}{\partial t} + \boldsymbol{\nabla} \cdot (\rho \boldsymbol{u}) = 0 \tag{7}$$

$$\frac{\partial \rho \boldsymbol{u}}{\partial t} + \boldsymbol{\nabla} \cdot (\rho \boldsymbol{u}\boldsymbol{u} + p\underline{\boldsymbol{\delta}}) = \boldsymbol{\nabla} \cdot \underline{\boldsymbol{\tau}} \tag{8}$$

$$\frac{\partial E}{\partial t} + \boldsymbol{\nabla} \cdot [(E + p)\boldsymbol{u}] = \boldsymbol{\nabla} \cdot (\underline{\boldsymbol{\tau}} \cdot \boldsymbol{u} - \boldsymbol{q_c} - \boldsymbol{q_d}) \tag{9}$$

Here, p, ρ, and E are pressure, density, and total energy, $\boldsymbol{u}$, $\boldsymbol{q}_c$, and $\boldsymbol{q}_d$ are mass-averaged velocity, heat conduction, and enthalpy flux, $\underline{\boldsymbol{\tau}}$ is the viscous stress tensor, and $\underline{\boldsymbol{\delta}}$ is the unit tensor. Crucially [14], the inclusion of an interdiffusional enthalpy flux term $\boldsymbol{q_d}$ in the energy equation describes the contribution of the diffusional flux $\boldsymbol{J}_i$ of species i with specific enthalpy h_i, number density n_i, molecular mass m_i, and drift velocity $\boldsymbol{w}_i$ relative to the mass-averaged mean velocity $\boldsymbol{u}$:

$$\boldsymbol{q_d} = \sum_{i=1}^{N} h_i \boldsymbol{J}_i$$

$$\boldsymbol{J}_i = n_i m_i \boldsymbol{w}_i$$

$$\boldsymbol{w}_i = \boldsymbol{u} - \boldsymbol{u}_i$$

The diffusional flux is calculated by a five-moment, first-order Chapman-Enskog binary collision model for ionized gas mixtures [15], which holds for the neutral case considered here. Several representative profiles of helium mass fraction and temperature at the argon-helium interface are given in Fig. 3.

3.2 Comparison with Proposed Correction

The adiabatic mixing assumption proposed in Section 2 is tested against the simulation data. Specifically, for each simulation time step the pure gas (helium and argon) temperatures are determined from the simulation temperature field. The adiabatic mixing rule is then used to calculate temperature as a function of the helium mole fraction. For validation, an ideal gas equation of state is used to be consistent with the simulation. Only the center vertical slice (at $x = 0.125$ m) of the simulation volume is used to be more representative of RMI experiments.

A comparison of the simulation temperatures and adiabatic temperatures as a function of the helium mole fraction is shown in Fig. 4, and the distribution of the deviation from the adiabatic mixing assumption is shown in Fig. 5. The adiabatic assumption shows good validity for both the post-shock and reshock conditions. The shape of the temperature profile calculated with the adiabatic mixing assumption matches the average simulated temperature to within about 30 K at worst, and about 20 K in general at any point along the curve. Unsurprisingly, the error following reshock is larger than the post-shock condition.

The validity of the approximation is evident in the error histogram in Fig. 5. The histograms are calculated only for points within the mixing layer. Specifically, if any component has a mole fraction larger than 99%, the data point is ignored. For both the

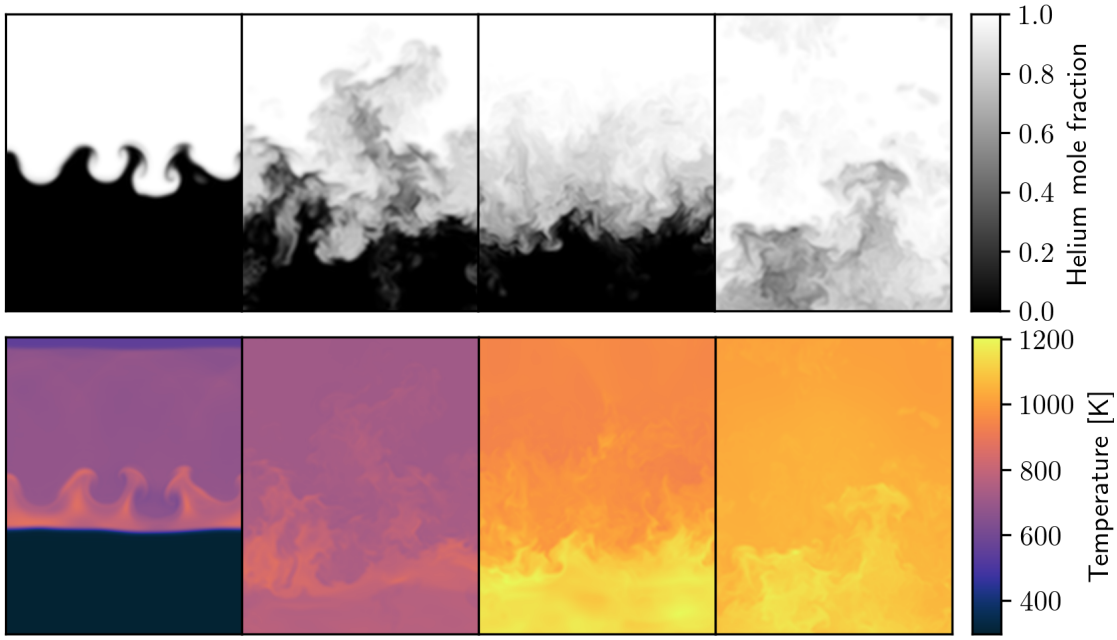

Fig. 3: Simulated helium mole fraction and temperature (from left to right) after initial shock interaction, prior to reshock, immediately after reshock, and after arrival of the rarefaction wave (at $t = 0.1$, 2.5, 3.0, and 5.5 ms after shock arrival).

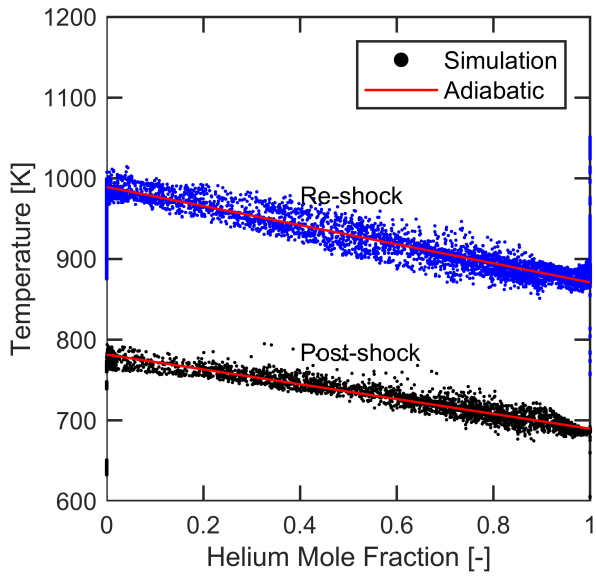

Fig. 4: Distribution of simulated temperatures (points) with adiabatic mixing rule superimposed (lines) at post-shock and reshock conditions.

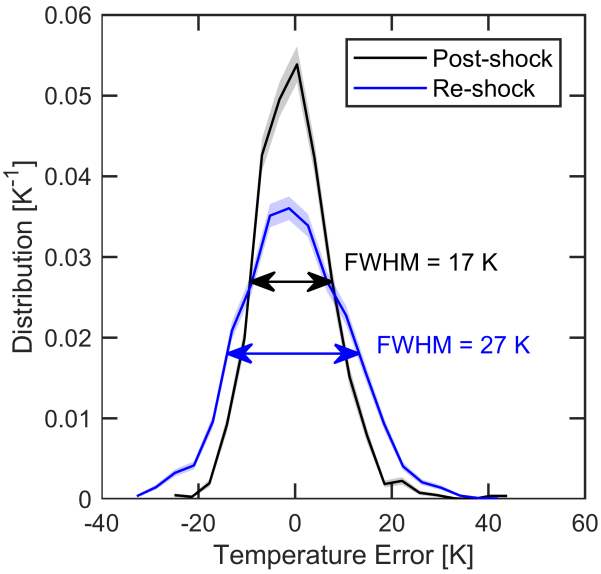

Fig. 5: Distribution functions of estimated temperature error resulting from adiabatic mixing assumption for post-shock (blue) and reshock (black) cases.

post-shock and reshock condition, the mean error is approximately 0 K. However, the root-mean-square error is 8 and 11 K for post-shock and reshock, respectively. Some of this error may be a result of uncertainty in the temperature of the unmixed argon and helium. Although ideally conditions are uniform outside of the mixing layer, this is not perfectly true as significant nonuniformity can be seen in the simulation results following reshock (see Fig. 6). This is likely a result of additional wave interactions, which slightly invalidates the assumption of uniform temperature in the unmixed regions.

One additional consideration before applying this correction to experimental data is the magnitude of thermal diffusion. Although advective processes are likely dominant due to the large velocities present in the flow, thermal diffusion may not be entirely negligible. Thermal diffusion results in energy transfer due to temperature nonuniformity in the flow field, and results in a non-adiabatic mixing process. Mathematically the diffusion contribution to energy transport is proportional to the temperature Laplacian ($\mathrm{D}E/\mathrm{D}t \propto \nabla^2 T$). The influence of thermal diffusion can be observed by comparing the adiabatic temperature error (*i.e.,* the difference between the actual and adiabatic temperature) to the temperature Laplacian. This is shown in Fig. 7 for a single time slice following reshock. From the plot, it is evident the temperature error and the Laplacian are moderately correlated over the entire sample, with a correlation coefficient of $r = -0.51$. This suggests that thermal diffusion could account for a significant portion of the non-adiabatic behavior. Further, there appears to be no relationship between temperature error and helium mole fraction.

4 Application to RMI Reshock Experiments

The proposed data correction procedure was applied to a series of acetone PLIF images taken at high speed (20 kHz) following reshock in a vertical shock tube at WiSTL. The facility configuration is described in detail in [8]. The initial condition consists of a helium-argon interface, in which the helium was seeded with acetone at 3.5% mole fraction. A

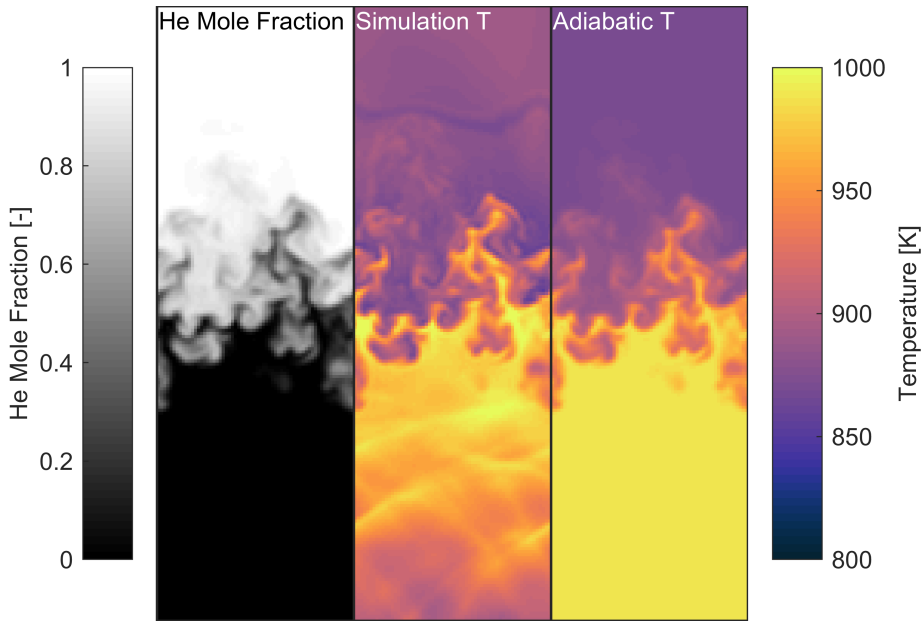

Fig. 6: Sample simulated mole fraction (left) and temperature field (middle) compared with adiabatic calculation (right). Pure argon is indicated by the black region in the mole fraction map, while white indicates pure helium.

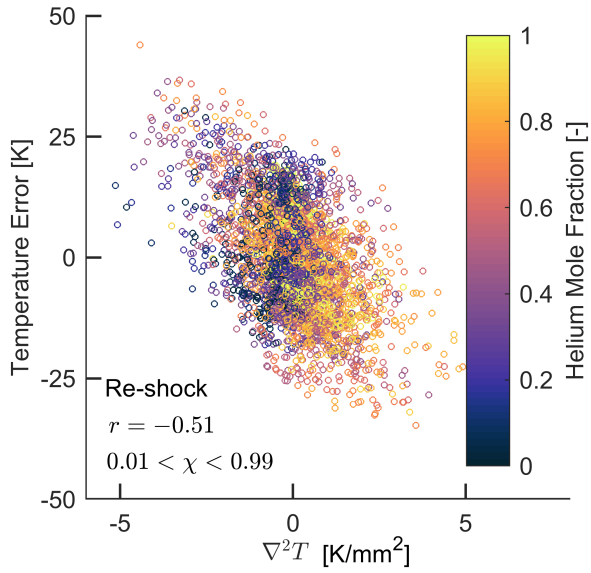

Fig. 7: Calculated temperature error (simulation temperature minus adiabatic temperature) as a function of the temperature Laplacian for a single reshock time. Data point color indicates the helium mole fraction.

perturbation was introduced on the interface by helium and argon jets on the side of the shock tube.

Acetone PLIF was excited using an all diode-pumped pulse-burst laser built at the University of Wisconsin, which provided approximately 30 mJ/pulse of laser energy at 266 nm and 20 kHz. The acetone fluorescence was captured by a Vision Research Phantom V1840 high-speed digital CMOS camera operated in Standard Binned mode with an integration duration of 1 μs. The camera was equipped with a 50 mm Nikon Nikkor f/1.2 lens and a set of filters that transmit light from approximately 300 to 524 nm. The camera was synchronized directly to the laser timing generator, and both systems were operated at 20 kHz after being triggered. Extensive camera characterization was performed prior to testing to assess camera linearity and noise characteristics, and this data was used to correct for non-linearity in the sensor response before applying PLIF corrections.

A set of 12 piezoelectric pressure transducers track the location of the shock wave and were used to measure the wave speed. Acetone concentration was measured from the exponential decay of fluorescence signal intensity in a uniform temperature region above the mixing layer from acetone PLIF imaging. The measured acetone concentration and measured wave speeds were then used to calculate the Mach number and upstream post-shock and reshock conditions. Since the acetone absorption cross-section is slightly temperature dependent, this process must be repeated until a self-consistent acetone concentration is achieved. Currently, only reshock was considered in this process, and the effect of expansion and compression waves following reshock were ignored.

Additionally, due to the presence of leaks in the system, some air was present in addition to helium/acetone and argon. The air mole fraction was estimated using the same one-dimensional gas-dynamics process. For the data presented here, the air mole fraction was estimated at approximately 20% and temperatures of the unmixed helium and argon regions were estimated to be 850 K and 1250 K, respectively.

The assumption of constant acetone mass was assessed with kinetic simulations at the expected reshock conditions using Cantera [16] and the Lawrence Livermore National Laboratory (LLNL) detailed n-heptane reaction mechanism [9]. Based on the results of the simulation, no more than 10% (relative) acetone dissociation is expected at the latest image times (10 ms following reshock) at 1200 K. At more typical conditions of 1000 K or less, no more than 1% (relative) dissociation is expected at any image timing.

PLIF images were corrected as described in Sec. 2 using the unmixed fluid temperatures and compositions estimated from one-dimensional gas-dynamics relations. The ideal gas equation of state was believed to be sufficient and is used for the data presented here; the Peng-Robinson equation of state [17] (with parameters taken from [18]) was additionally tested and observed to have a negligible effect on the adiabatic mixing calculation. Fluorescence quantum yield and absorption cross-section are initially assumed to be constant, and Eq. (3) is evaluated to determine an approximate local number density. The estimated number density is then used in the adiabatic mixing calculation to determine temperature and photophysical parameters for each pixel. The calculation is repeated until the temperature and number density calculations converge. This procedure typically takes only a few iterations.

A series of corrected concentration, adiabatic temperature, and raw PLIF signal intensity images from a single experiment are shown in Fig. 8. The procedure used does not filter out contributions due to the laser sheet profile and some striations are visible in the mixture fraction and temperature images. These could be removed with the application of a band-rejection filter. However, the majority of striations are removed by the PLIF

correction and should not influence the results significantly. The remaining striations are likely due to error in the correction process or beam-steering due to large density fluctuations at the interface.

Comparing Fig. 8 to Fig. 6, it is clear that the calculation when applied to experimental data produces a nonuniform temperature above the mixing layer. Although the simulation does show temperature nonuniformity in this region, the simulated temperature nonuniformity occurs at constant composition and is not a result of mixing. Since the experimental temperature is assumed to be a result of mixing, the calculated mole fraction and temperature in this region are erroneous. Experimentally, temperature variation results in nonuniform PLIF intensity which is interpreted as variation in mole fraction, and leads to a small error in mole fraction and a mixture fraction less than unity. As a result of the adiabatic mixing assumption, the calculated temperature is higher than the unmixed helium temperature. Since the local temperature nonuniformity in this region is the result of another mechanism besides turbulent mixing processes (this region must be 'pure' as it is above the mixing layer), the temperature calculated in this region contains errors.

For the data presented here, the 'pure' fluid temperatures and compositions have been estimated from one-dimensional gas-dynamics, using pressure transducers to determine wave speed. Although this is commonly done to measure wave velocities (in, *e.g.*, [19, 20]), additional assumptions are required to determine post-shock and reshock properties for the two fluids. This could be a significant source of error for temperature correction or estimation using an adiabatic mixing assumption.

Finally, the calculated helium fraction is compared to the case where temperature and composition are assumed to be constant. Constant temperature and composition fixes the fluorescence quantum yield and absorption cross-section such that only the Beer-Lambert attenuation correction is performed. The span-wise averaged helium mass and mole fractions are shown in Fig. 9. The mass fractions are calculated using the same composition estimated for Fig. 8. As noted in Fig. 9, the proposed correction results in a longer tail towards the unseeded heavy gas side which corresponds to a very low signal region (approximately 20 - 50 counts) immediately below the interface. This is unsurprising since the PLIF signal intensity is expected to be very weak at high temperature, and thus a weak PLIF signal can correspond to a non-negligible acetone concentration. This tail is also observable in Fig. 8, particularly at the latest time, immediately below the interface. It is not presently clear whether this tail is a result of the mixing process, acetone diffusion from helium to argon, or experimental error. It should be noted that errors in the FQY and absorption cross section models could also amplify this tail. Additionally, the proposed correction produces a higher helium concentration measurement above the mixing layer, implying lower rates of pre-shock diffusive mixing.

5 Conclusions

A method for correcting PLIF data for analysis of high-speed turbulent mixing and especially for analysis of RMI has been outlined. The method employs an adiabatic mixing assumption within the mixing layer to estimate local temperature. Previous PLIF modeling work has been leveraged to use the temperature estimate to rigorously correct PLIF images and determine corrected local mole fractions. The adiabatic mixing assumption has been validated against simulation data and found to be reasonable within the mixing layer. Outside of the mixing layer, wave interactions can result in additional tempera-

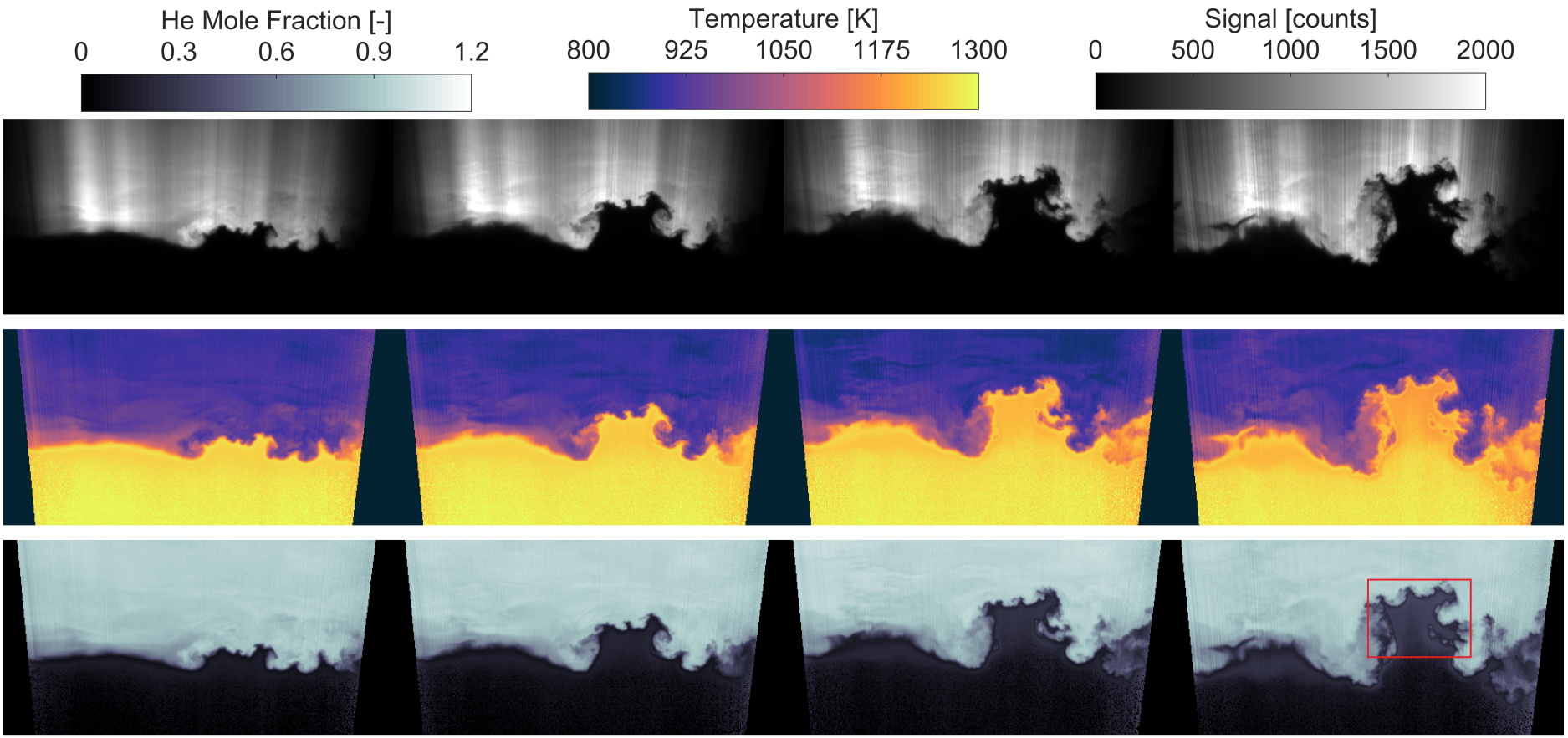

Fig. 8: Series of raw PLIF intensity (top), adiabatic temperature (middle), and helium mole fraction (bottom) for four images each separated by 200 μs. The red box in the bottom right image indicates a long 'tail' observed in the calculated helium mole fraction.

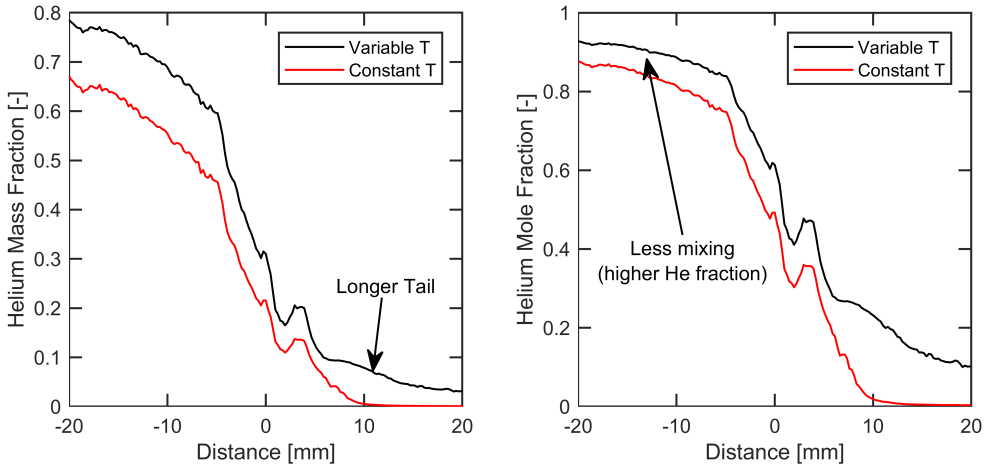

Fig. 9: Span-wise averaged helium mass fraction (left) and mole fraction (right) calculated for a single experimental image following reshock using the proposed adiabatic mixing approach (black) and constant property (red) approach.

ture variation that does not originate from turbulent mixing. The correction has been demonstrated on high-speed acetone PLIF data taken following reshock of a helium-argon interface, and mixture fraction and temperature maps have been produced for this data set. The adiabatic mixing calculation requires knowledge of the unmixed fluid compositions and temperatures that can be estimated from one-dimensional gas-dynamics, but this could be a large source of uncertainty in the calculation. The corrected experimental data show significant differences in local mixing compared to results only corrected for Beer-Lambert attenuation, demonstrating the importance of correcting for PLIF temperature and composition dependence.

References

[1] C.-N. Yeh et al., SAE Transactions, 1156 (1994)
[2] W. Hwang et al., SAE Technical Paper 2007-01-4130 (2007)
[3] S. Kaiser and C. M. White, SAE International Journal of Engines **1**, 657 (2009)
[4] A. W. Cook, Physics of Fluids **19**, 055103 (2007)
[5] R. K. Hanson et al., *Spectroscopy and optical diagnostics for gases* (Springer, 2016)
[6] B. Collins and J. W. Jacobs, Journal of Fluid Mechanics **464**, 113 (2002)
[7] S. Wang et al., The Journal of Physical Chemistry A **119**, 7257 (2015)
[8] D. T. Reese et al., Journal of Fluid Mechanics **849**, 541 (2018)
[9] M. Mehl et al., Proceedings of the Combustion Institute **33**, 193 (2011)
[10] M. Thurber and R. K. Hanson, Applied Physics B **69**, 229 (1999)
[11] J. D. Koch et al., Journal of Quantitative Spectroscopy and Radiative Transfer **109**, 2037 (2008)
[12] M. Löffler et al., Applied Optics **49**, 37 (2010)
[13] J. D. Koch et al., Applied Optics **43**, 5901 (2004)
[14] A. W. Cook, Physics of Fluids **21**, 055109 (2009)
[15] R. Schunk, Planetary and Space Science **23**, 437 (1975)

[16] D. G. Goodwin et al., *Cantera: an object-oriented software toolkit for chemical kinetics, thermodynamics, and transport processes*, `https://www.cantera.org`, Version 2.4.0, 2018
[17] D.-Y. Peng and D. B. Robinson, Industrial & Engineering Chemistry Fundamentals **15**, 59 (1976)
[18] R. C. Reid et al., *The properties of gases and liquids* (McGraw Hill Book Co., New York, NY, 1987)
[19] C. Weber et al., Physics of Fluids **24**, 074105 (2012)
[20] B. Balakumar et al., Journal of Fluid Mechanics **696**, 67 (2012)